Iron-rich clay mineral synthesis using design of experiments approach

Hella Boumaiza, Patrick Dutournie, Jean-Marc Le Meins, Lionel Limousy, Jocelyne Brendle, Christelle Martin, Nicolas Michau, Liva Dzene

This is a post-peer-review, pre-copyedit version of an article published in *Applied Clay Science*. The final authenticated version is available online at: https://doi.org/10.1016/j.clay.2020.105876

IRON-RICH CLAY MINERAL SYNTHESIS USING DESIGN OF EXPERIMENTS APPROACH

Hella Boumaiza[a], Patrick Dutournié[a], Jean-Marc Le Meins[a], Lionel Limousy[a], Jocelyne Brendlé[a], Christelle Martin[b], Nicolas Michau[b] and Liva Dzene[a,*]

[a]Institut de Science des Matériaux de Mulhouse CNRS UMR 7361, Université de Haute-Alsace, Université de Strasbourg, 3b rue Alfred Werner, 68093 Mulhouse CEDEX, France

[b]Andra, R&D Division, Packages and Materials Department, 1/7 rue Jean Monnet, F-92298 Châtenay-Malabry CEDEX, France

*liva.dzene@uha.fr

Abstract

The precipitation of iron-rich clay minerals has been reported in various geologic environments. However, large quantities of these minerals are not widely accessible to study their thermodynamic properties and thus improve our understanding of these particular geological systems. To obtain sufficient amount of iron-rich minerals, their synthesis can be foreseen. A design of experiments and surface response methodology was used in this study to find optimum synthesis conditions for these clay minerals. Three parameters were considered: quantity of OH^-, synthesis time and temperature. The quantity of OH^- had the largest influence on the synthesis result. The amount of 2:1 type clay mineral with respect to 1:1 type clay mineral increased with OH/Fe molar ratio. Time and temperature had less significant impact on the synthesis outcome, yet the formation of 2:1 type phase was favored at short synthesis time (1 day) and high temperature (160°C). The findings suggested that the kinetic of 2:1 type clay

mineral phase formation with respect to 1:1 type phase was faster, yet the precipitation was strongly dependent on the availability of the reactants.

Key words

iron-rich clay minerals, design of experiments, synthesis, nontronite, berthierine

Introduction

Clay minerals are layered silicate materials, where silica tetrahedra are arranged in continuous sheet combined with hexagonally coordinated metal-containing octahedral sheet. In general, two types of structures can be distinguished, a so-called 2:1 type clay mineral where the metal-containing octahedral sheet is sandwiched between two silicate sheets forming a 2:1 layer, and a 1:1 type clay mineral, where one silicate sheet is combined with one octahedral sheet forming a 1:1 layer (Figure 1). These minerals are widely encountered in natural sedimentary rocks and soils. The most common elements found in natural clay minerals are Si, Al, Mg, Fe, O and H (i.e., montmorillonite, beidellite, vermiculite, kaolinite, saponite). Minerals containing solely Si, Fe, O and H are known, but less common (i.e., greenalite, cronstedtite, hisingerite, nontronite).

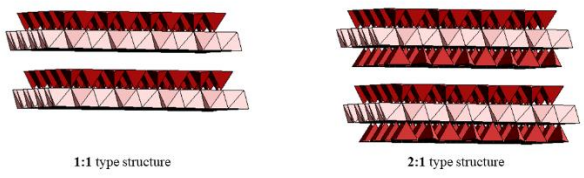

Figure 1. Schematic representation of clay mineral structures.

The environments where the formation of iron-rich clay minerals have been reported include deep-sea sediments (Baldermann et al., 2015; Tosca et al., 2016), subduction zones (Beaufort et al., 2015; Sforna et al., 2018), transform faulting (Kodolányi et al., 2012), the surface of Mars (Chemtob et al., 2015) and meteorites (Zolotov, 2015). Their presence has also been reported at the interface between different materials such as steel and glass (Schlegel et al., 2016) and steel and clay-rich rocks (Lanson et al., 2012) studied for the conception of radioactive waste repository sites.

For the different geological systems, it is of great interest to predict the evolution of these systems whether millions of years in the past, as in the case of Mars and Earth surfaces, or other thousands of years in the future as in the case of long-term radioactive waste repository sites. In order to do this, geochemical modelling is required to predict the evolution with time of the mineralogical composition of these different systems. The prediction of this evolution is crucial as it enables assessing the changes of key properties such as porosity and permeability.

To assess the clay mineral thermodynamic properties for geochemical modelling, different approaches were developed (Tardy and Fritz, 1981; Vieillard, 2000). The thermodynamic properties of clay minerals are particularly challenging to constrain owing to the great chemical and structural variability of these minerals (Gailhanou et al., 2013). A common approach to assess them is the summation of oxide/hydroxide parameters, which on the other hand are well-known. However, the knowledge of experimental thermodynamic and kinetic properties of iron-rich clay minerals would enhance the robustness of the models, as well as allow the comparison of experimental data with modelling (Gailhanou et al., 2013).

As Fe-rich clay mineral phases and especially tri-octahedral ones are seldom encountered in environments and as only very small quantities can be extracted, their synthesis can be foreseen. Two reviews have recently gathered the different methods carried out to prepare iron-rich clay minerals (Dzene et al., 2018; Petit et al., 2017). The hydrothermal synthesis route remains the

preferred one because it is a versatile and easy to use process which allows the attainment of well crystallized compounds (Jaber et al., 2013; Kloprogge, 1998; Le Forestier et al., 2010; Reinholdt et al., 2005). The key parameters governing the formation of clay minerals are the sources of reactants, synthesis time, temperature and the pH of the hydrogel. Regarding the preparative methods, the formation of a sol followed by a gel is expected to yield a homogeneous repartition of elements in the final product (Dzene et al., 2018). The use of Fe^{2+} source for the preparation of precursor is expected to increase the kinetics of synthesis and to allow obtaining faster a well-crystallized product compared to the use of Fe^{3+} source (Petit et al., 2017). The three other parameters, pH, time and temperature, have been widely varied in literature and no particular tendency can be extracted. Thus, the variation from neutral to alkaline pH has been previously reported, and syntheses have been performed in various time and temperature ranges. Nevertheless, the three later parameters can significantly influence the type of synthesized clay mineral and its crystallinity (Jaber et al., 2013; Kloprogge et al., 1999). For this reason, the three parameters (time, temperature and the initial quantity of OH^-) were chosen as the variables for this study. In general, time will intervene in reaction kinetics and crystal growth processes. The increase of synthesis time will allow attaining the equilibrium or pseudo-equilibrium conditions and will allow growing larger crystals. The temperature will intervene in both, in reaction kinetics and thermodynamics. On the one hand the increase of temperature is expected to accelerate the kinetics of reaction. Thus, higher temperature would lead to shorter synthesis time. On the other hand, the increase of temperature will influence the thermodynamics of the reaction. As the precipitation of clay minerals is in general an endothermic process (Giffaut et al., 2014), the increase of the temperature is expected to favor the formation of products. Finally, the quantity of OH^- will influence the condensation reactions (Cundy and Cox, 2005).

The complexity of the studied reactions, make the systematic exploration rather challenging. Therefore, the design of experiments (DOE) can be used. This approach largely applied in natural sciences and engineering has been only recently explored in the synthesis of inorganic materials such as zeolite, aluminophosphate and glass (Carvalho et al., 2013; Cichocki and Kościelniak, 1999; Ji et al., 2014; Katovic et al., 2001; Zhang et al., 2009). This approach has allowed to eliminate insignificant parameters and reveal the most significant ones, which influence material properties such as crystallinity, ion exchange capacity and solubility of the product. However, the method has not yet been explored for lamellar silicate synthesis. This might be due to the fact, that the characterization of synthesis products requires a set of several analytical techniques, thus choosing the response variable(s) for the DOE is not trivial. By using oriented preparation for X-ray diffraction, we took advantage of a particular feature of lamellar materials to characterize them. The objective of this study then is to test this characterization technique for the design of experiments and explore in an efficient way, how, the three parameters: quantity of OH^-, synthesis time and temperature, influence the type of synthesized clay mineral and its crystallinity.

Materials and methods

2.1. Design of experiments

Preliminary experiments identified the three parameters that influence the type and amount of obtained clay mineral: synthesis time t, temperature T and $(OH/Fe)_{ini}$ molar ratio. They allowed also to set the relevant range of each of these three parameters (T=80 °C – 180 °C, t=1 - 7 days and $(OH/Fe)_{ini}$=2 - 4) for the design of experiments. To analyze the results in terms of synthesis parameters, a methodology based on Design Of Experiments (DOE) and Response Surface Methodology (RSM) was used (Myers et al., 2016).

For this, a central composite design for k = 3 factors (T, t, $(OH/Fe)_{ini}$) was used (Anderson and Whitcomb, 2016). It consists of three sets of experimental points: 2^k points coming from classical factorial design (two levels), 2k axial points ("star points") and a center point, i.e. 8+6+1 experimental tests in this case (Figure 2). Thus, the central point in our study is [130 °C; 4 days; $(OH/Fe)_{ini}$=3]. The eight points (factorial points) define the domain of the study, which is also the domain of the validity to consider for the numerical interpretation of results, i.e. (T=100 °C -160 °C, t=2.3 - 5.7 days) and $(OH/Fe)_{ini}$=2.4 - 3.6). The "star points" are additional points required to increase the efficiency of the quadratic fitting.

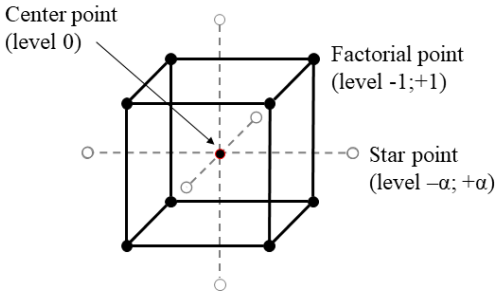

Figure 2. Scheme representing central composite design for k=3 factors.

The main objective of DOE is to obtain the maximum of information from a minimum of experiments. RSM enables to explore relationships between the studied functions and the operating factors. To obtain an optimal response a linear quadratic model with 10 parameters is used to numerically approximate the response function. For this, a system of 15 equations with 10 variables is statistically solved by minimizing a quadratic criterion, i.e. $\sum_{i=1}^{n}\left(y_{exp}(i) - y_{calc}(i)\right)^2$, where y_{exp} and y_{calc} are the experimental and calculated variable, respectively. The studied parameters (T, t and OH/Fe molar ratio) are standardized in the range [-1,1] to analyze the sensitivity of the calculated response functions. Additional experiments were performed to investigate experimental error. The relevance of the response functions

(presented in paragraph 2.3.) was studied by statistical analysis via the calculation of five criteria, as follows:

- The determination coefficient r^2

- The standard error of estimate $S = \sqrt{\frac{\sum_{i=1}^{n}\left(y_{exp}(i)-y_{calc}(i)\right)^2}{n-6}}$

- The Marquard's percent standard deviation $MPSD = \sqrt{\frac{1}{n-6}\sum_{i=1}^{n}\frac{\left(y_{exp}(i)-y_{calc}(i)\right)^2}{y_{exp}(i)^2}}$

- The mean absolute error $EABS = \frac{1}{n}\sum_{i=1}^{n}\left|y_{exp}(i) - y_{calc}(i)\right|$

- The mean relative error $RE = \frac{1}{n}\sum_{i=1}^{n}\left|\frac{y_{exp}(i)-y_{calc}(i)}{y_{exp}(i)}\right|$

The five criteria are used to assess the pertinence of the numerical approximation. The studied functions are studied directly and in power, logarithmic, exponential, hyperbolic, etc. forms. According to the five studied criteria, the best function is chosen and used for the numerical approximation.

2.2. Synthesis protocol and chemicals used

The following chemicals were used: iron (II) sulfate heptahydrate ($FeSO_4 \cdot 7H_2O$, Merck, 99.9 %) as Fe(II) source, fumed silica (SiO_2, Aerosil® 380, Evonik) as silicon source, sodium hydroxide (NaOH, Sigma Aldrich, 97 wt.%) to provide an alkaline medium and sodium dithionite ($Na_2S_2O_4$, Sigma Aldrich, ca. 85 wt.%,) to maintain reducing conditions. Double distilled water (DDW, 18.2 MΩ·cm) was used for all the experiments.

The procedure is based on a hydrothermal synthesis starting from a suspension having an Fe to Si molar ratio equal to 1.5. The procedure consisted of dissolving successively in 70 mL of distilled water 0.041 g of $Na_2S_2O_4$, 4.510 g of $FeSO_4 \cdot 7H_2O$, 0.647 g of SiO_2 and a given quantity

of NaOH at the desired OH/Fe molar ratio corresponding to each run of experiment (Table 1). Thus, the initial theoretical concentrations were $c(Fe^{2+}) = 0.23$ mol·L^{-1}, $c(Si)=0.15$ mol·L^{-1} and $c(OH^-)=0.45 – 1.00$ mol·L^{-1}. The mixture was stirred during 2 hours at room temperature before being sealed in a Teflon-lined stainless-steel autoclaves (Top Industrie ®, 150 mL) and put at the desired temperature (T) ranging from 80 °C to 180 °C and time (t) ranging from 1 to 7 days. After the synthesis, the autoclaves were cooled down at room temperature. The run products were then recovered and washed by centrifugation (8000 rpm for 10 min), and dried at 60 °C.

2.3. Choice of response for the design of experiments

Clay minerals are highly anisotropic, therefore, it is challenging to obtain truly un-oriented sample for powder XRD. To overcome this drawback, oriented preparations can be made, recording solely (00ℓ) reflections, which are characteristic for different clay mineral types. An example of X-ray diffractogram of oriented preparation is shown in Figure 3. Thus, 1:1 type structure would have $d_{(001)}$ value of ca. 7 Å and 2:1 type structure would have $d_{(001)}$ value in the range of 10 Å to 15 Å.

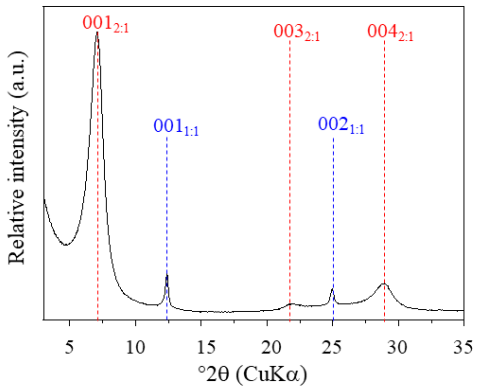

Figure 3. Example of XRD pattern of oriented preparation (Run N°01). Red dashed lines indicate (00ℓ) plane reflections of 2:1 type clay mineral and blue dashed lines indicate (00ℓ) plane reflections of 1:1 type clay mineral.

The absence of other (*hkℓ*) plane reflections was systematically checked in the analyzed samples. The measured peak areas of different phases then represent the relative abundance of each phase in the sample. Moreover, it is also possible to assess the information regarding the coherent scattering domain size (CSDS) in the direction perpendicular to the corresponding (00ℓ) plane. In conventional powder X-ray diffraction, this information can be obtained from the Full Width at Half Maximum (FWHM) of a reflection. However, in this particular case of oriented preparations, the simplifications can be done so that the peak intensity can provide this information on the CSDS in the direction perpendicular to the corresponding (00ℓ) plane. The chosen synthesis protocol revealed the formation of both types of clay minerals (1:1 and 2:1). The assumption was made that the chemical composition of 2:1 type phase is very similar in all samples and the chemical composition of 1:1 type phase is very similar in all samples. The objective of the study was to find optimum synthesis conditions for each type of phase. For this reason, the area and intensity ratios of (001) reflection, (respectively R(A) and R(I)), between 1:1 and 2:1 type structures were chosen as the studied responses in the design of experiments (Figure 4).

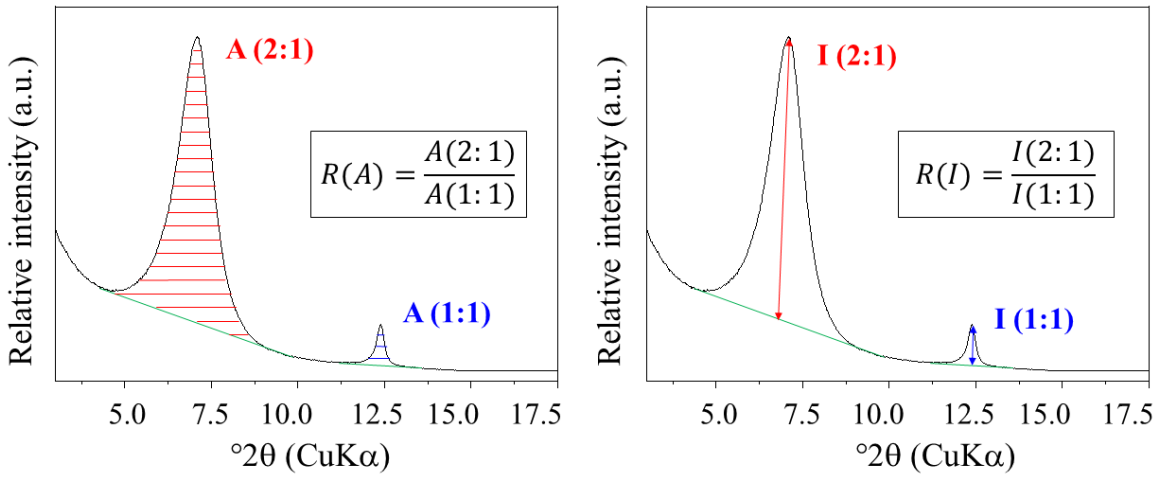

Figure 4. Illustration of R(A) and R(I) between 1:1 and 2:1 type clay minerals.

2.4. X-ray diffraction

The mineralogical composition of the samples and, more specifically, the type of clay mineral was determined using X-ray diffraction of powder and oriented preparations. The powders were previously ground and then introduced into PMMA sample holder with a cavity 25 mm in diameter and 1.2 mm deep, whereas the thin films of oriented samples were prepared from diluted suspensions by deposition onto a glass slide. All the samples, powder and oriented, were characterized on a Bruker D8 Advance X-ray diffractometer with a LYNXEYE XE-T high resolution energy dispersive 1-D detector ($CuK\alpha_{1,2}$) fully opened (2.938°). This kind of detector allows to avoid Fe fluorescence effects with Cu X-ray tube.

For the powder samples, the X-ray diffractograms were recorded from 3° to 70° 2θ at a step scan of 0.017° 2θ, a step time of 1.80 s with variable divergence slits that ensure that the irradiated sample length (*i.e.*, 15 mm) is kept equal over a measured range of 2θ. For the oriented samples, the XRD patterns were recorded in the range from 3 to 40° 2θ at a step scan of 0.017° 2θ, a step time of 3.3 s with a fixed divergence slits width of 0.08°. For both kind of samples (powder and oriented), automatic motorized anti-scatter screen is used for effective suppression of air-scatter at low angles 2θ.

Results

3.1. Experiments used for modelling

Examples of powder XRD patterns for selected experiments are given in Figure 5. The experimental synthesis conditions corresponding to each run N° are reported in Table 1. The formed reaction products were not pure phases, but containing also iron oxides: hematite and magnetite/maghemite. Two sets of experiments were performed in order to extract the optimal conditions to obtain a single type of clay mineral. The first set of experiments was designed

considering the central composite model. It contained a minimal number of experiments equal to 15 performed for OH/Fe molar ratio [2.0 – 4.0].

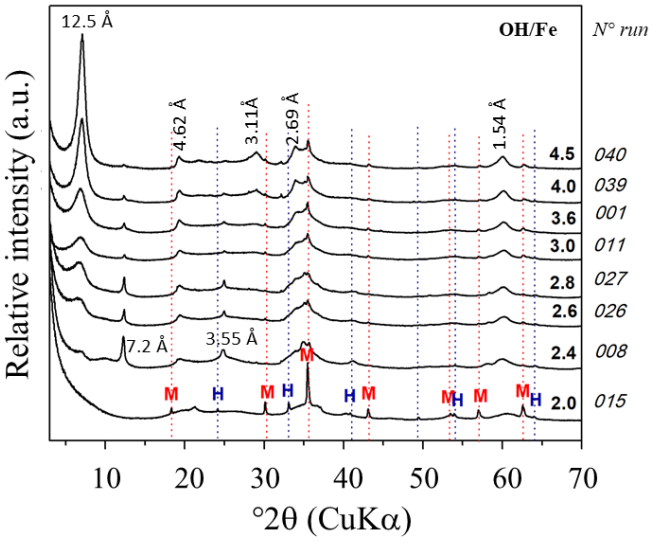

Figure 5. Powder XRD patterns of selected experiments. For the experimental conditions corresponding to each run N° see Table 1.

The first set of experiments produced satisfactory results in the validity range (2.4 – 3.6, i.e. standardized parameters = +1 / -1), but the errors increased significantly at the boundaries of the studied range (r^2 = 0.94 for OH/Fe = [2.4 – 3.6] and 0.89 for OH/Fe = [2 – 4]). The addition of a second set was consequently necessary in order to extract the optimal conditions from the quadratic equation. In fact, when calculating the extracted responses R(A) and R(I), different tendencies were noticed between the experiments performed for high OH/Fe molar ratios [2.4 – 4.0] in comparison with the lower values [2.0 – 2.4]. The studied response could therefore not be estimated based on the same model. The second set of experiment was then focused on high OH/Fe ratios, up to 4.5, and the linear quadratic model was studied accordingly in the range [2.4 – 4.5]. In order to improve the relevance of the model, 4 tests were added (N°26, N°27, N°39 and N°40) for the calculation of R(A) and R(I).

Table 1. Experimental conditions and obtained R(I) and R(A) corresponding to each run.

Set	Run N°	T (°C)	$(OH/Fe)_{ini}$	t (days)	R(I)	R(A)
1	01	160	3.6	2.3	6.9	29.2
	01-R				13.1	44.3
	02	160	2.4	2.3	0.1	1.2
	03	100	3.6	2.3	5.3	15.9
	04	100	2.4	2.3	0.2	2.0
	05	130	3.0	1.0	2.1	8.3
	06	130	3.0	7.0	1.4	5.9
	07	160	3.6	5.7	3.0	11.2
	08	160	2.4	5.7	0.2	0.4
	09	100	3.6	5.7	2.5	10.1
	10	100	2.4	5.7	0.9	5.1
	11	130	3.0	4.0	2.5	10.7
	11-R1				3.9	18.1
	11-R2				2.8	13.0
	12	180	3.0	4.0	1.1	6.0
	13	80	3.0	4.0	7.4	17.0
	14	130	4.0	4.0	13.1	31.8
	15	130	2.0	4.0	-	-
2	16	150	3.0	7.0	0.6	11.4
	26	130	2.6	5.0	0.8	3.5
	26-R				0.9	4.1
	27	130	2.8	5.0	0.6	3.5
	39	180	4.0	1.0	24.6	64.8
	40	180	4.5	1.0	32.1	68.2

4 runs (N°01-R, N°11-R1, R2 and N°26-R) were repeated to investigate the experimental error. These tests were chosen to have an experiment corresponding to predominant 2:1 type clay mineral (test N°01), an experiment resulting in a majority of 1:1 type clay mineral (test N°26) and an experiment with intermediate proportions of 2:1 and 1:1 type clay minerals (test N°11). The obtained experimental error was important but all the repeated tests show a parallel trend. The relevance of RSM is studied on the basis of all the experimental tests. In the run N°15, which was repeated several times, the only crystalline phases identified were iron oxides. No crystalline clay minerals were identified in powder XRD pattern (Figure 5) of this run, thus no values of R(A) and R(I) could be obtained for oriented preparations.

236 3.2. Study of response function R(A): ratio between relative quantities of 2:1 and 1:1 clay
237 minerals

238 This function is proportional to the relative quantity of each phase in the sample. The obtained
239 quadratic model for the studied function R(A) is given below (eq. 1). The analysis of sensitivity
240 of the quadratic model for R(A) shows that the response function is highly dependent on OH/Fe
241 molar ratio (coefficients before linear $\frac{\overline{OH}}{Fe}$, square $\frac{\overline{OH}^2}{Fe}$ and coupled $\bar{T} \times \frac{\overline{OH}}{Fe}$ variables). In the
242 same way, linear, quadratic and coupled coefficients relative to time are relatively small, unlike
243 the coupled coefficient $\bar{T} \times \bar{t}$.

244 $$\ln(\mathrm{R(A)}) = 2.292 - 0.268\bar{T} - 0.059\bar{T}^2 + 1.275\frac{\overline{OH}}{Fe} - 0.46\frac{\overline{OH}^2}{Fe} - 0.062\bar{t} - 0.064\bar{t}^2 +$$

245 $$0.409\,\bar{T} \times \frac{\overline{OH}}{Fe} - 0.143\bar{T} \times \bar{t} - 0.059\,\frac{\overline{OH}}{Fe} \times \bar{t} \qquad \text{(eq.1)}$$

246 The pertinence of the model is investigated from all trials (20) except run N°15. Averages of
247 tests N°01, N°11 and N°26 are used for the calculation of all the tests for the experimental error.

248 $r^2 = 0.961$, S = 4.706, MPSD = 0.512, EABS = 2.754, RE = 0.308

249 Figure 6 shows the area ratio versus temperature for different times for a low OH/Fe molar ratio
250 (Figure 6A), an average OH/Fe molar ratio (Figure 6B) and a high OH/Fe molar ratio (Figure
251 6C). The function increases significantly with OH/Fe molar ratio while it increases with time
252 at low temperature and decreases at high temperature. The same applies for temperature, since
253 an increase of temperature decreases the area ratio except for high OH/Fe molar ratio values.
254 The model represents well experimentally observed tendencies. Considering the significant
255 experimental error, the tendencies given by the model are the same as for the experimental
256 points thus validating the obtained model.

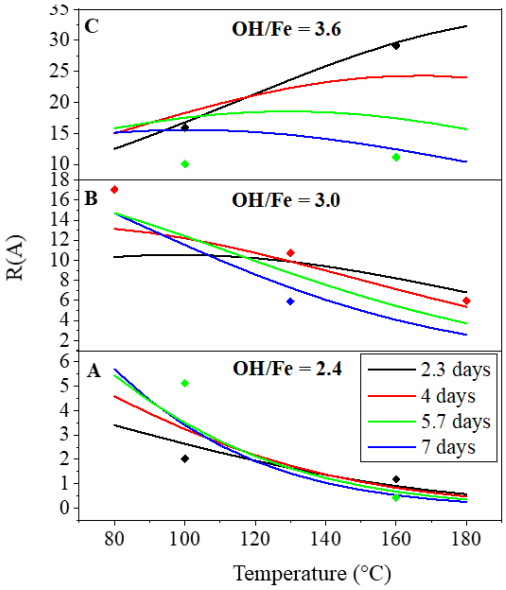

257

258 **Figure 6.** Time and temperature influence on the obtained R(A) for $(OH/Fe)_{ini}$ molar ratios
259 equal to 2.4 (A), 3.0 (B) and 3.6 (C). Diamonds represent experimental points from Table 1,
260 Set I.

261 For illustration, selected XRD patterns of oriented preparations are given in Figure 7. In
262 agreement with results obtained from R(A) investigation, it can be seen that the initial (OH/Fe)
263 molar ratio significantly influences the type of clay mineral obtained. For low $(OH/Fe)_{ini}$ molar
264 ratios the formation of 1:1 type clay mineral is favored, whereas for high $(OH/Fe)_{ini}$ molar ratios
265 the 2:1 type clay mineral phase is dominant. The relative quantity of 2:1 clay mineral (with
266 respect to 1:1 type clay mineral) increases significantly with $(OH/Fe)_{ini}$.

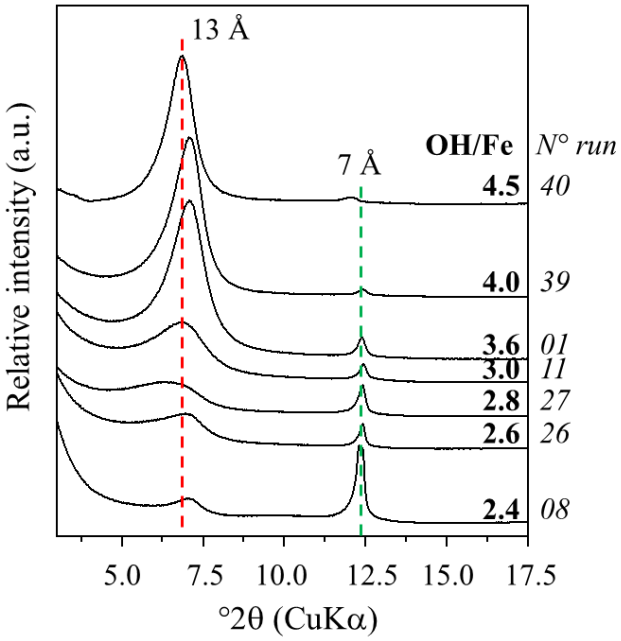

Figure 7. XRD patterns of oriented preparations for selected experiments (red dashed line 2:1 clay mineral type, green dashed line 1:1 type). For the experimental conditions corresponding to each run N° see Table 1.

3.3. Study of phase abundance and crystallinity: response function R(I)

This response function gives additional quantitative information and results about crystallinity. For R(I) (eq.2), it is noted that the conclusions about the sensitivity analysis are almost the same, except for time contribution, which is, in this present case, more significant, especially, the coupled terms with temperature and initial OH/Fe molar ratio. Indeed, the diffracted intensity in the particular case of oriented preparations among other factors also includes the contribution of the size of coherent scattering domain. It is expected that the synthesis time influences the size of formed particles, and thus the coherent scattering domain (Carrado et al., 2006). Thus, the contribution of time in the function of R(I) being more important than in R(A) function is in agreement with expected results.

$$R(I) = 2.146 - 0.283\bar{T} + 0.531\bar{T}^2 + 3.127\frac{\overline{OH}}{Fe} + 1.100\frac{\overline{OH}^2}{Fe} - 0.734\bar{t} - 0.141\bar{t}^2 + 0.928\,\bar{T} \times \frac{\overline{OH}}{Fe} - 0.819\bar{T} \times \bar{t} - 1.834\frac{\overline{OH}}{Fe} \times \bar{t} \qquad \text{(eq.2)}$$

The pertinence of the model is investigated from all trials (20):

$r^2 = 0.962$, S = 2.014, MPSD = 3.232, EABS = 1.403, RE = 1.422

For high OH/Fe molar ratio, i.e. $(OH/Fe)_{ini}$ = 3.6, it has to be underlined that whatever the temperature T, R(I) decreases with time (Figure 8). Likewise, the temperature increases the contribution of time on R(I) (Figure 8B). That is to say, the ratio of diffracted peak intensity increases with respect to the background (with no curvature, see Figure 4) without the increase of peak full-width at half-maximum when time decreases and temperature increases. It leads then to a conclusion that 2 :1 type clay mineral phase formation is favored in short times, and this becomes even more important with the increase of temperature.

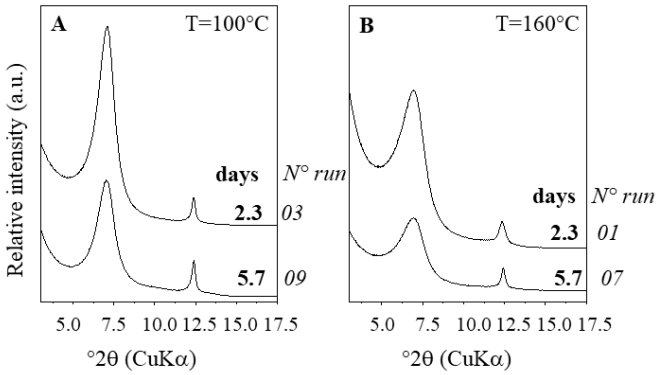

Figure 8. XRD patterns of oriented preparations obtained for $(OH/Fe)_{ini}$ molar ratio = 3.6 at two different temperatures T=100°C (A) and T=160°C (B) for two different times of 2.3 and 5.7 days (Runs N° 01, N°03, N°07 and N° 09 *cf.* Table 1).

With this function (R(I)), the interpretation is limited for results obtained with low initial OH/Fe molar ratio because R(I) is close to zero (Table 1). To overcome this drawback, the last response

298 function (1 /R(I)) was defined and studied to investigate the favoring of 1:1 type clay formation.
299 All the studied parameters influence this function and no contribution can be neglected (eq.3).

300 $$\ln\left(1+\frac{1}{R(I)}\right) = 0.453 + 0.188\bar{T} - 0.019\bar{T}^2 - 0.726\frac{\overline{OH}}{Fe} + 0.386\frac{\overline{OH}}{Fe}^2 - 0.060\bar{t} + 0.058\bar{t}^2 -$$

301 $$0.217\,\bar{T} \times \frac{\overline{OH}}{Fe} + 0.139\bar{T} \times \bar{t} + 0.267\,\frac{\overline{OH}}{Fe} \times \bar{t} \qquad \text{(eq.3)}$$

302 The pertinence of the model is investigated from 18 trials (set 1 + tests N°26 and N°27):

303 $r^2 = 0.981$, S = 0.472, MPSD = 1.192, EABS = 0.310, RE = 0.621

304 Starting from these 3 mathematical models, optimal solutions are searched by minimizing an
305 objective function.

306 3.4 Optimum parameters favoring the 2:1 type clay mineral formation

307 The study of the favored formation of 2:1 type clay mineral requires to investigate the
308 parameters (T, time and initial OH/Fe molar ratio) resulting in high values of R(A) and R(I). It
309 was considered that R(A) > 30 and R(I) > 12 (objective functions) are representative values of
310 investigated conditions. Figure 9 shows in a temperature / time diagram the optimal solutions
311 for having a vast majority of 2:1 type clay for R(A) > 30 (Figure 9A) and for R(I) > 12 (Figure
312 9B) for $(OH/Fe)_{ini}$ = [3.6 – 4.0]. The objective function is reached in the hatched area. This
313 objective (R(A) > 30) is reached for high OH/Fe molar ratio and especially for short synthesis
314 time and high temperature. The same trend is observed for R(I) with temperature but the
315 influence of time is more moderate at low temperatures below 120 °C.

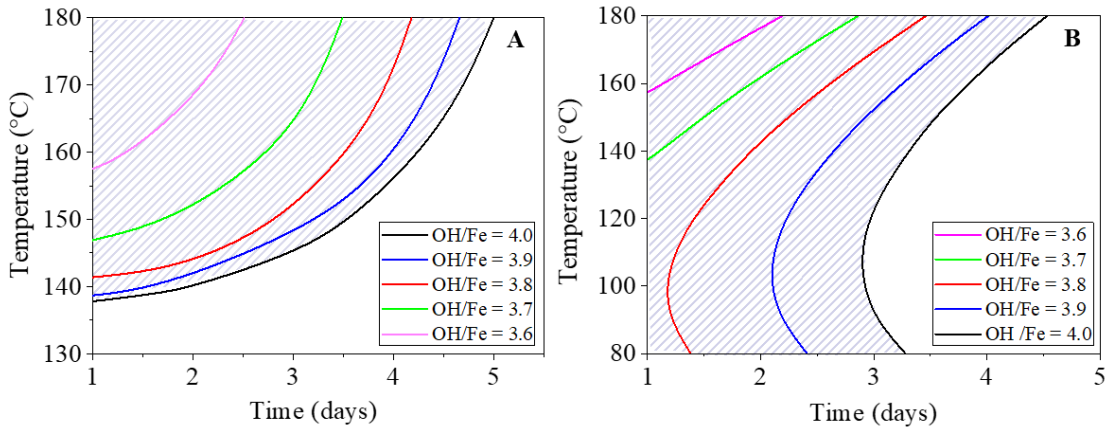

316

317 **Figure 9.** Conditions of temperature and time favoring the formation of the 2:1 type clay
318 mineral with R(A)> 30 (A) and for R(I) > 12 (B) for $(OH/Fe)_{ini}$ = [3.6 – 4.0].

319 3.5 Optimum parameters favoring the 1:1 type clay mineral formation

320 The favored formation of 1:1 type clay mineral, corresponding to the very low values of R(A)
321 and R(I) is studied with response function (1/R(I)). It was considered that 1/R(I) > 2 are
322 representative values of investigated conditions. It was not possible to fix a higher value for
323 1/R(I) > 2 due to the experimental error. This objective is reached, when OH/Fe molar ratio is
324 as low as possible, i.e., OH/Fe=2.4 (Figure 10). It is important to mention, that at OH/Fe < 2.2,
325 the formation of crystalline 1:1 type clay mineral phase was not observed (Table 1).

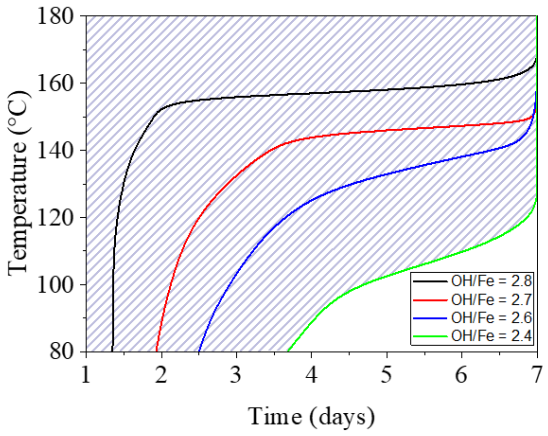

326

Figure 10. Conditions of temperature and time favoring the formation of the 1:1 type clay mineral with $1/R(I) > 2$ for $(OH/Fe)_{ini} = [2.4 – 2.8]$.

The optimal conditions for the formation of 1:1 type clay mineral phase (with respect to 2:1 phase) are reached for short time and high temperature. Interestingly, the formation of 1:1 type clay mineral phase can also be achieved at low temperature (below 140 °C) and short times (less than 3 days) with low OH/Fe molar ratio. In comparison, the synthesis of 2:1 phase is favored only at high temperatures and high OH/Fe molar ratio. This aspect can be relevant to environmentally friendly synthesis procedure, as less resources (chemicals and energy) are consumed.

Discussion

The observed tendencies in this study are in agreement with previously reported studies. Indeed, Fe-serpentines (1:1 type clay mineral) were observed for the experiments at low temperatures below 150°C (Bertoldi et al., 2005; Lantenois et al., 2005; Pignatelli et al., 2014; Rivard et al., 2013; Tosca et al., 2016), whereas Fe-rich chlorites (2:1 type clay mineral) were identified at higher temperature of 300 °C (Mosser-Ruck et al., 2016). However, it has to be noted that in other studies the duration of experiments was different. The experiments reported in Pignatelli et al. (2014) lasted 6 months and the experiment of Mosser-Ruck et al. (2016) went for 25 months. Also, in these experiments additional phenomena were in operation such as the dissolution of iron from metallic plates, which could have been the limiting step regarding the precipitation of clay mineral phase.

It can be expected that the formation of phyllosilicate phases is strongly governed by sol-gel process as in the case of other silicates such as zeolites. An important step is the precipitation of dissolved silicon. This condensation reaction is strongly governed by the amount of hydroxyl ions (Cundy and Cox, 2005). Then, it is not surprising that the quantity of OH^- has the most

significant impact on both studied functions. It has been noted previously that Si speciation in solution, influence the structure of synthesized nontronite (2:1 type clay mineral) (Baron et al., 2016). In a similar way here, the quantity of OH^- acts on the species and their amount in solution during the synthesis. Also, the study of Tosca et al. (2016) notes the influence of pH. They performed the study at three different pH (7.0,7.5 and 8.0), and they noted that the concentration of Fe^{2+} and SiO_2 in solution decreased faster when pH increased. Thus, the precipitation of greenalite-like phase occurred faster when pH increased. Although the pH in our study was very different (13 to 14) compared to the study of Tosca et al. (2016), both studies note the important influence of this parameter towards the precipitation of clay minerals.

For synthesis at high OH/Fe ratio, a high temperature favors the formation of 2:1 type clay mineral. Indeed, the thermodynamic constant of the precipitation reaction increases with temperature and favors the formation of clays (enthalpy of precipitation reactions being positive) (Giffaut et al., 2014). In the same way, the reaction kinetics increase with the increase of temperature and the preferential precipitation of 2:1 type clay mineral can be attributed to a faster kinetic. It is in agreement with observations reported in the study of Grubb (1971), which used 1N NaOH solution in his experiments and observed that minnesotaite (2:1 type clay mineral) become the dominant constituent in the three year experiments. Nevertheless, in our study, when synthesis time increases this tendency is reversed (R(A) decreases) possibly due to a limited species (intermediate reaction leading to the precipitation of 2:1 phase clay mineral). This indicates a decrease of the ratio R(A) but the amounts can probably increase.

For synthesis performed at low OH/Fe ratios, the quantity of OH^- is limited. There is no thermodynamic limitation but the kinetics are decreased by the limiting reactant. The reaction leading to the precipitation of 2:1 type clay mineral is favored at high pH and disfavored in these operating conditions. So, the reaction of precipitation of 1:1 phase clay mineral becomes dominating.

To summarize, the ratio of reaction kinetics ($k_{2:1}$ / $k_{1:1}$) increases with temperature and decreases when the available amount of hydroxyl ion in solution decreases. This amount of hydroxyl ion decreases as the precipitation reactions advances (time dependent).

Conclusion

The feasibility of synthesis of 2:1 and 1:1 type clay minerals was demonstrated at given physicochemical conditions. Depending on these conditions, the synthesis can be tailored towards favoured formation of one or another type of phases. To optimize the number of experiments and the amount of information, which can be extracted from them, a design of experiments was used. From few synthesis experiments, the predominant operating parameters and the conditions leading to the formation of 2:1 and 1:1 type clay minerals were identified. From RSM (Response Surface Methodology) investigations the optimal conditions of synthesis were estimated for each type of phase.

Among the studied parameters (synthesis temperature, time and ratio OH/Fe), the ratio OH/Fe (proportional to the available amount of hydroxyl ions in solution) is preponderant. At high OH/Fe ratio, the precipitation of 2:1 type clay mineral is favoured with respect to 1:1 type clay mineral. The decrease of available hydroxyl ions with time slowed down the kinetic. For the same reason, the formation of 1:1 type clay mineral was favoured when the availability of hydroxyl ions decreased (low OH/Fe ratio).

From these results, synthesis of several grams of desired products will be carried out to perform detailed characterizations (full set of thermodynamic properties, different spectroscopic measurements, structural model …). These investigations will allow to improve the understanding of many aspects related to the presence of either or both 2:1 and 1:1 type iron bearing clays in natural or anthropized environments: identification of each type of phases in experimental products or natural samples, understanding of their neoformation mechanisms,

sensitivity to relevant or discriminant physico-chemical parameters, thermos-kinetic modelling of geochemical systems.

Acknowledgments

The study was conducted within the framework of R&D project between the French National Agency for Radioactive Waste Management (ANDRA) and Institut Carnot MICA.

References

Anderson, M.J., Whitcomb, P.J., 2016. RSM Simplified: Optimizing Processes Using Response Surface Methods for Design of Experiments, 2nd ed. CRC Press.

Baldermann, A., Warr, L.N., Letofsky-Papst, I., Mavromatis, V., 2015. Substantial iron sequestration during green-clay authigenesis in modern deep-sea sediments. Nat. Geosci. 8, 3–8. https://doi.org/10.1038/ngeo2542

Baron, F., Petit, S., Tertre, E., Decarreau, A., 2016. Influence of Aqueous Si and Fe Speciation on Tetrahedral Fe(III) Substitutions in Nontronites: a Clay Synthesis Approach. Clays Clay Miner. 64, 230–244. https://doi.org/10.1346/CCMN.2016.0640309

Beaufort, D., Rigault, C., Billon, S., Billault, V., Inoue, A., Inoue, S., Patrier, P., 2015. Chlorite and chloritization processes through mixed-layer mineral series in low-temperature geological systems – a review. Clay Miner. 50, 497–523. https://doi.org/10.1180/claymin.2015.050.4.06

Bertoldi, C., Dachs, E., Cemic, L., Theye, T., Wirth, R., Groger, W., 2005. The Heat Capacity of the Serpentine Subgroup Mineral Berthierine (Fe2.5Al0.5)[Si1.5Al0.5O5](OH)4. Clays Clay Miner. 53, 380–388. https://doi.org/10.1346/CCMN.2005.0530406

Carrado, K.A., Decarreau, A., Petit, S., Bergaya, F, Lagaly, G, 2006. Chapter 4 Synthetic Clay Minerals and Purification of Natural Clays, in: Bergaya, Faïza, Theng, B.K.G., Lagaly, Gerhard (Eds.), Handbook of Clay Science. Elsevier, 115–139. https://doi.org/10.1016/S1572-4352(05)01004-4

Carvalho, M.M., Ruotolo, L.A.M., Fernandez-Felisbino, R., 2013. Synthesis of aluminophosphate by the ionothermal method using factorial design. Microporous Mesoporous Mater. 165, 163–167. https://doi.org/10.1016/j.micromeso.2012.08.020

Chemtob, S.M., Nickerson, R.D., Morris, R. V., Agresti, D.G., Catalano, J.G., 2015. Synthesis and structural characterization of ferrous trioctahedral smectites: Implications for clay mineral genesis and detectability on Mars. J. Geophys. Res. Planets 120, 1119–1140. https://doi.org/10.1002/2014JE004763

Cichocki, A., Kościelniak, P., 1999. Experimental designs applied to hydrothermal synthesis of zeolite ERI+OFF(T) in the Na2O-K2O-Al2O3-SiO 2-H2O system: Part 2. Regular study. Microporous Mesoporous Mater. 29, 369–382. https://doi.org/10.1016/S1387-1811(99)00006-2

Cundy, C.S., Cox, P.A., 2005. The hydrothermal synthesis of zeolites: Precursors, intermediates and reaction mechanism. Microporous Mesoporous Mater. 82, 1–78. https://doi.org/10.1016/j.micromeso.2005.02.016

Dzene, L., Brendlé, J., Limousy, L., Dutournié, P., Martin, C., Michau, N., 2018. Synthesis of iron-rich tri-octahedral clay minerals: A review. Appl. Clay Sci. 166, 276–287. https://doi.org/10.1016/j.clay.2018.09.030

Gailhanou, H., Blanc, P., Rogez, J., Mikaelian, G., Horiuchi, K., Yamamura, Y., Saito, K., Kawaji, H., Warmont, F., Grenèche, J.-M., Vieillard, P., Fialips, C.I., Giffaut, E.,

445 Gaucher, E.C., 2013. Thermodynamic properties of saponite, nontronite, and vermiculite
446 derived from calorimetric measurements. Am. Mineral. 98, 1834–1847.
447 https://doi.org/10.2138/am.2013.4344

448 Giffaut, E., Grivé, M., Blanc, P., Vieillard, P., Colàs, E., Gailhanou, H., Gaboreau, S., Marty,
449 N., Madé, B., Duro, L., 2014. Andra thermodynamic database for performance
450 assessment: ThermoChimie. Appl. Geochemistry 49, 225–236.
451 https://doi.org/10.1016/j.apgeochem.2014.05.007

452 Grubb, P.L.C., 1971. Silicates and their paragenesis in the brockman iron formation of
453 Wittenoom Gorge, Western Australia. Econ. Geol. 66, 281–292.
454 https://doi.org/10.2113/gsecongeo.66.2.281

455 Jaber, M., Komarneni, S., Zhou, C.-H., 2013. Synthesis of Clay Minerals, in: Bergaya, F.,
456 Lagaly, G. (Eds.), Handbook of Clay Science Fundamentals. Elsevier, 223–241.
457 https://doi.org/10.1016/B978-0-08-098258-8.00009-2

458 Ji, L., Si, Y., Liu, H., Song, X., Zhu, W., Zhu, A., 2014. Application of orthogonal
459 experimental design in synthesis of mesoporous bioactive glass. Microporous
460 Mesoporous Mater. 184, 122–126. https://doi.org/10.1016/j.micromeso.2013.10.007

461 Katovic, A., Cosco, M., Cozzucoli, P., Giordano, G., 2001. The factorial experimental design
462 applied to the zeolite synthesis, in: Colella, C., Coluccia, S., Gamba, A. (Eds.), Studies in
463 Surface Science and Catalysis 140. Elsevier Science B.V., pp. 323–330.
464 https://doi.org/10.1016/S0167-2991(01)80161-0

465 Kloprogge, J.T., 1998. Synthesis of smectites and porous pillared clay catalysts: a review. J.
466 Porous Mater. 5, 5–41. https://doi.org/10.1023/A:1009625913781

467 Kloprogge, J.T., Komarneni, S., Amonette, J.E., 1999. Synthesis of smectite clay minerals: A

468 critical review. Clays Clay Miner. 47, 529–554.
469 https://doi.org/10.1346/CCMN.1999.0470501

470 Kodolányi, J., Pettke, T., Spandler, C., Kamber, B.S., Ling, K.G., 2012. Geochemistry of
471 ocean floor and fore-arc serpentinites: Constraints on the ultramafic input to subduction
472 zones. J. Petrol. 53, 235–270. https://doi.org/10.1093/petrology/egr058

473 Lanson, B., Lantenois, S., van Aken, P.A., Bauer, A., Plancon, A., 2012. Experimental
474 investigation of smectite interaction with metal iron at 80°C: Structural characterization
475 of newly formed Fe-rich phyllosilicates. Am. Mineral. 97, 864–871.
476 https://doi.org/10.2138/am.2012.4062

477 Lantenois, S., Lanson, B., Muller, F., Bauer, A., Jullien, M., Plançon, A., 2005. Experimental
478 study of smectite interaction with metal Fe at low temperature: 1. Smectite
479 destabilization. Clays Clay Miner. 53, 597–612.
480 https://doi.org/10.1346/CCMN.2005.0530606

481 Le Forestier, L., Muller, F., Villieras, F., Pelletier, M., 2010. Textural and hydration
482 properties of a synthetic montmorillonite compared with a natural Na-exchanged clay
483 analogue. Appl. Clay Sci. 48, 18–25. https://doi.org/10.1016/j.clay.2009.11.038

484 Mosser-Ruck, R., Pignatelli, I., Bourdelle, F., Abdelmoula, M., Barres, O., Guillaume, D.,
485 Charpentier, D., Rousset, D., Cathelineau, M., Michau, N., 2016. Contribution of long-
486 term hydrothermal experiments for understanding the smectite-to-chlorite conversion in
487 geological environments. Contrib. to Mineral. Petrol. 171, 1–21.
488 https://doi.org/10.1007/s00410-016-1307-z

489 Myers, R.H., Montgomery, D.C., Anderson-Cook, C.M., 2016. Response Surface
490 Methodology: Process and Product Optimization Using Designed Experiments, 4th ed.

491 John Wiley & Sons, Inc.

492 Perronnet, M., Jullien, M., Villiéras, F., Raynal, J., Bonnin, D., Bruno, G., 2008. Evidence of
493 a critical content in Fe(0) on FoCa7 bentonite reactivity at 80°C. Appl. Clay Sci. 38,
494 187–202. https://doi.org/10.1016/j.clay.2007.03.002

495 Petit, S., Baron, F., Decarreau, A., 2017. Synthesis of nontronite and other Fe-rich smectites :
496 a critical review. Clay Miner. 52, 469–483.
497 https://doi.org/10.1180/claymin.2017.052.4.05

498 Pignatelli, I., Bourdelle, F., Bartier, D., Mosser-Ruck, R., Truche, L., Mugnaioli, E., Michau,
499 N., 2014. Iron-clay interactions: Detailed study of the mineralogical transformation of
500 claystone with emphasis on the formation of iron-rich T-O phyllosilicates in a step-by-
501 step cooling experiment from 90°C to 40°C. Chem. Geol. 387, 1–11.
502 https://doi.org/10.1016/j.chemgeo.2014.08.010

503 Reinholdt, M., Miehé-Brendlé, J., Delmotte, L., Le Dred, R., Tuilier, M.-H., 2005. Synthesis
504 and characterization of montmorillonite-type phyllosilicates in a fluoride medium. Clay
505 Miner. 40, 177–190. https://doi.org/10.1180/0009855054020164

506 Rivard, C., Montargès-Pelletier, E., Vantelon, D., Pelletier, M., Karunakaran, C., Michot, L.J.,
507 Villieras, F., Michau, N., 2013. Combination of multi-scale and multi-edge X-ray
508 spectroscopy for investigating the products obtained from the interaction between
509 kaolinite and metallic iron in anoxic conditions at 90 °C. Phys. Chem. Miner. 40, 115–
510 132. https://doi.org/10.1007/s00269-012-0552-6

511 Schlegel, M.L., Martin, C., Brucker, F., Bataillon, C., Blanc, C., Chorro, M., Jollivet, P.,
512 2016. Alteration of nuclear glass in contact with iron and claystone at 90°C under anoxic
513 conditions: Characterization of the alteration products after two years of interaction.
514 Appl. Geochemistry 70, 27–42. https://doi.org/10.1016/j.apgeochem.2016.04.009

515 Sforna, M.C., Brunelli, D., Pisapia, C., Pasini, V., Malferrari, D., Ménez, B., 2018. Abiotic
516 formation of condensed carbonaceous matter in the hydrating oceanic crust. Nat.
517 Commun. 9. https://doi.org/10.1038/s41467-018-07385-6

518 Tardy, Y., Fritz, B., 1981. An ideal solid solution model for calculating solubility of clay
519 minerals. Clay Miner. 361–373.

520 Tosca, N.J., Guggenheim, S., Pufahl, P.K., 2016. An authigenic origin for Precambrian
521 greenalite: Implications for iron formation and the chemistry of ancient seawater. Geol.
522 Soc. Am. Bull. 128, 511–530. https://doi.org/10.1130/B31339.1

523 Vieillard, P., 2000. A new method for the prediction of Gibbs free energies of formation of
524 hydrated clay minerals based on the electronegativity scale. Clays Clay Miner. 48, 459–
525 473. https://doi.org/10.1346/CCMN.2000.0480406

526 Zhang, D., Wang, R., Yang, X., 2009. Application of fractional factorial design to ZSM-5
527 synthesis using ethanol as template. Microporous Mesoporous Mater. 126, 8–13.
528 https://doi.org/10.1016/j.micromeso.2009.03.015

529 Zolotov, M.Y., 2015. Formation of brucite and cronstedtite-bearing mineral assemblages on
530 Ceres. Icarus 228, 13–26. https://doi.org/10.1016/j.icarus.2013.09.020